Available online at https://link.springer.com/journal/42241
http://www.jhydrodynamics.com
Journal of Hydrodynamics, 2021, 33(5): 970-978
https://doi.org/10.1007/s42241-021-0086-9

Heat transfer and flow structure of two-dimensional thermal convection over ratchet surfaces *

Cheng Wang[1], Lin-feng Jiang[1], He-chuan Jiang[1], Chao Sun[1, 2], Shuang Liu[1, 3]
1. *Center for Combustion Energy, Key Laboratory for Thermal Science and Power Engineering of Ministry of Education, Department of Energy and Power Engineering, Tsinghua University, Beijing 100084, China*
2. *Department of Engineering Mechanics, School of Aerospace Engineering, Tsinghua University, Beijing 100084, China*
3. *Yau Mathematical Sciences Center, Tsinghua University, Beijing 100084, China*

(Received April 19, 2021, Revised July 4, 2021, Accepted August 17, 2021, Published online November 8, 2021)

Abstract: This paper presents a numerical study of the Rayleigh-Bénard convection (RBC) in two-dimensional cells with asymmetric (ratchet) roughness distributed on the top and bottom surfaces. We consider two aspect ratios of roughness $\gamma = 1, 2$ and the range of the Rayleigh number $1.0\times10^6 \le Ra \le 2.0\times10^{10}$ with the Prandtl number $Pr = 4$. The influences of the roughness on the heat transfer and the flow structure are found to be strongly dependent on both Ra and the roughness geometry. We find that the roughness can have a significant influence on the organization of the secondary corner rolls, and the corner rolls are evidently suppressed by the roughness for intermediate values of Ra. In the presence of the roughness, a sharp jump of the Nu values is identified as the Ra value is slightly increased, accompanied with the dramatic changes of the large-scale flow structure and the plume dynamics. The influences of the ratchet orientation on the heat transfer and the flow structure are discussed and analyzed.

Key words: Turbulent convection, ratchet roughness, heat transfer, flow structure

Introduction

The thermal convection is a widespread phenomenon in nature, as well as in industry. Examples include the convections in the atmosphere and the ocean and in the ventilation systems. A classical model for the thermal convection is the Rayleigh-Bénard convection (RBC) model, which consists of a fluid layer heated from below and cooled from above[1-4]. The RBC is controlled by two primary dimensionless parameters, the Rayleigh number Ra and the Prandtl number Pr, which are defined as:

$$Ra = \frac{\alpha g \Delta H^3}{\nu\kappa}, \quad Pr = \frac{\nu}{\kappa} \tag{1}$$

where g is the gravity acceleration, Δ is the temperature difference between the bottom and top plates, H is the height of the convective cell, and α, ν, κ are the thermal expansion coefficient, the kinematic viscosity, and the thermal diffusivity of the fluid, respectively. Besides Ra, Pr, there is also a geometric parameter, the aspect ratio γ of the convection cell. A key response parameter of the RBC is the global heat transfer, which is measured by the Nusselt number

$$Nu = \frac{Q}{k\Delta/H} \tag{2}$$

where Q is the total heat flux across the fluid layer, k is the thermal conductivity of the fluid. One fundamental task of the turbulent convection studies is to predict the Nu values as a function of the control parameters (Ra, Pr and γ)[1-4]. At given values of Pr, γ, the $Nu(Ra)$ dependence is generally expressed in an effective power law, $Nu \sim Ra^{\lambda}$.

Most studies of the RBC were focused on

* Projects supported by the Natural Science Foundation of China (Grant Nos. 11988102, 91852202), the China Postdoctoral Science Foundation (Grant No. 2019M660614).
Biography: Cheng Wang (1997-), Male, Ph. D. Candidate,
E-mail: wangc19@mails.tsinghua.edu.cn
Corresponding author: Shuang Liu,
E-mail: liushuang9012@mail.tsinghua.edu.cn

idealized systems with smooth confining boundaries. But the boundaries of natural convection systems are generally not smooth, it is of great interest to study the convection over rough surfaces from both the fundamental and practical points of view. The roughness can have a significant influence on the flow properties of the turbulent thermal convection and is an efficient way to enhance the heat transfer, which is of practical value to the thermal management in industrial processes. In the past decades, the RBC over rough surfaces was extensively studied. It was shown that the roughness can significantly increase the heat transfer by enhancing the plume emission[5-7]. Besides the Nu value, it was reported that the roughness can increase the local scaling exponent λ in the $Nu(Ra)$ relation, as compared with the smooth case[8-16].

The effects of the roughness on the flow properties of the RBC are sensitive to the roughness geometric characteristics. The relative thicknesses of the boundary layers (BLs) and the roughness were shown to be critical factors for the heat transfer properties of the thermal convection over rough surfaces[11]. The local heat transfer scaling behavior can be manipulated by changing the aspect ratio of the rough elements, and a local $Nu \sim Ra^{1/2}$ scaling can be realized for the roughness with an optimal aspect ratio[10, 12-13]. At a higher value of Ra, the scaling exponent λ may saturate back to a value close to that in the smooth case. The appearance of the scaling-enhanced and saturated regimes can be understood in terms of the changes of the dissipation properties with the increase of Ra values[13]. In a numerical study of the two-dimensional thermal convection over the multi-scale roughness, Zhu et al.[15] observed the $Nu \sim Ra^{1/2}$ scaling over an extended Ra range. Interestingly, the roughness may also reduce the global heat transfer[17-18].

Although the thermal convection over rough surfaces has received a wide attention and a considerable understanding has been achieved, so far most studies have only considered the rough elements with a symmetric geometry, while the roughness on the natural and engineering surfaces is generally not very regular and is asymmetric. In a combined experimental and numerical study, Jiang et al.[19] examined the effects of the asymmetric (ratchet) roughness on the three-dimensional turbulent RBC for a fixed roughness shape. They found that the ratchet roughness can lock the orientation of the large-scale circulation (LSC) through the symmetry breaking when the system is perfectly leveled out, and the turbulent heat transfer is sensitive to the relative orientations of the LSC and the ratchet roughness. Further studies of the effects of the asymmetric roughness on the turbulent RBC are desirable due to the broad parameter space and the complexity of the problem.

Inspired by previous studies, this paper will explore how the heat transfer and the flow structures are manipulated through introducing the asymmetric, ratchet roughness structures using well-resolved two-dimensional numerical simulations. Two roughness aspect ratios are considered, and the effects of the ratchet roughness on the heat transfer and the flow structure are analyzed.

1. Numerical model

A sketch of the two-dimensional Rayleigh-Bénard cell is shown in Fig. 1. The cell consists of periodically arranged ratchet roughness on the top and bottom surfaces. The fluid motion is governed by the following dimensionless Navier-Stokes equations within the Boussinesq approximation:

$$\nabla \cdot \boldsymbol{u} = 0\,,\quad \frac{\partial \boldsymbol{u}}{\partial t} + \boldsymbol{u}\cdot\nabla\boldsymbol{u} = -\nabla p + \sqrt{\frac{Pr}{Ra}}\nabla^2\boldsymbol{u} + T\hat{k}\,,$$

$$\frac{\partial T}{\partial t} + \boldsymbol{u}\cdot\nabla T = \frac{1}{\sqrt{PrRa}}\nabla^2 T \qquad (3)$$

where $\boldsymbol{u} = (u, w)$ is the velocity vector in the horizontal and vertical directions (x, z), T is the temperature, and p is the pressure. The vector $\hat{k}$ denotes the unit vector pointing in the direction opposite to the gravity. The governing equations (3) are non-dimensionalized with respect to the cell height H, the free-fall velocity $U = \sqrt{\alpha g \Delta H}$, and the temperature drop Δ between the bottom and top surfaces. There are two dimensionless parameters in equations (3), the Rayleigh number Ra and the Prandtl number Pr, as defined in the first section. To complement the governing equations (3), the no-slip condition is employed for the velocity on all solid boundaries. For the temperature, we employ the isothermal condition on the rough top and bottom surfaces and the adiabatic condition on the sidewalls. In the simulations, the temperatures on the top and bottom surfaces are fixed at the values of 0, 1, respectively.

As shown in Fig. 1, the convective cell is of unit aspect ratio with $\Gamma = L/H = 1$. The triangular rough elements with the height h and the width l are uniformly distributed on the top and bottom surfaces with a vertex angle of 90°. In this study, the convection cell is clockwisely tilted by a small angle of $\beta = 6°$, such that the direction of the LSC can be

locked at the clockwise direction, and the relative orientation of the LSC and the ratchet roughness are fixed in each case[19]. We consider two roughness aspect ratios $\gamma = l/h = 1,\ 2$ with a fixed roughness height $h/H = 0.0625$. For $\gamma = 1,\ 2$, the numbers of the ratchet elements on each horizontal plate are $N_r = 16,\ 8$, respectively, and the contact areas of the roughness surface are 2.4, 1.6 times the area of the horizontal plate, respectively. For any given roughness shape, two different cases can be further distinguished based on how the fluid flow sweeps the roughness surface, as sketched in Figs. 1(b), 1(c). It is referred to case A (case B) when the LSC sweeps along the ratchet surface with a smaller (larger) slope. In the present work the Rayleigh number is varied in the range $10^6 \le Ra \le 2\times10^{10}$ at a fixed Prandtl number $Pr = 4$.

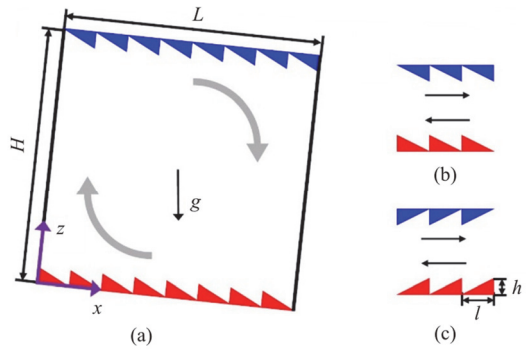

Fig. 1 (Color online) (a) Sketch of the two-dimensional Rayleigh-Bénard cell with asymmetric roughness on the top and bottom surfaces. The convection cell is clockwisely tilted at an angle $\beta = 6°$, resulting in a large-scale circulation locking in the clockwise direction. Two different roughness configurations can be further defined, which are denoted as (b) case A and (c) case B

The direct numerical simulations are performed based on the open-source code AFiD[20-21], which has been well verified and extensively used for the study of the turbulent convection over rough surfaces[13, 15, 19, 22]. Here we only present the essential elements of the numerical methods. The computational domain is discretized using a second-order center difference method on a staggered grid, and the time stepping is performed with a third-order Runge-Kutta scheme for the explicit terms combined with a Crank-Nicholson scheme for the implicit terms. The computational grid is stretched in the vertical direction and clustered near the horizontal plates to resolve the BLs. The immersed boundary method is employed to implement the roughness structures[23]. The details of the numerical methods can be found in Refs. [20-21].

Adequate grid resolution is used to resolve the small-scale flow structures in the bulk and the thin BLs near the walls. The thermal BLs are resolved with at least 10 grid points, to comply with the recommendation by Shishkina et al.[24]. In the case of the largest heat flux at $Ra = 2.0\times10^{10}$, $\lambda = 1$, a grid resolution of 2 560×2 560 is used. In this case we estimate the Kolmogorov and Batchelor scales by using the global criteria $\eta_K/H = Pr^{1/2}/[Ra(Nu-1)]^{1/4} = 1.25\times10^{-3}$, $\eta_B/H = \eta_K/\sqrt{Pr} = 6.25\times10^{-4}$. The maximal grid spacing Δ_g satisfies the relations $\Delta_g \le 0.47\eta_K$, $\Delta_g \le 0.94\eta_B$, which is sufficient for the present purpose. More numerical details are given in the appendix. As discussed in the first section, the global heat transfer is measured by the Nusselt number Nu, which is calculated by averaging the heat flux $\sqrt{RaPr}\langle wT\rangle_{x,t} - \langle \partial_z T\rangle_{x,t}$ through five horizontal planes at different vertical positions of the convection cell over at least 400 free-fall time units after the initial transients, where $\langle\cdot\rangle_{x,t}$ denotes averaging over a horizontal plane and over the time. The standard deviation of the averaged value of Nu from the five horizontal sections is less than 1%.

2. Results and discussions

We first examine how the heat transfer is affected by the ratchet roughness. The results of Nu values as a function of the Ra values are given in Fig. 2(a) in a log-log plot in both the smooth and rough cases. To better illustrate the variations of the Nu values, the data are shown in a compensated way in Fig. 2(b). It is found that the Nu value in the smooth case satisfies an effective scaling law $Nu \sim Ra^{0.30}$ over the Ra range considered, as is consistent with the results in the literature[25], while in a cell with roughness, $Nu(Ra)$ relation sees a much more complicated variation. At low values of Ra, the heat transfer is reduced in the rough cells compared with that in the smooth case, as was reported and systematically studied in Refs. [17-18]. The heat transfer reduction is due to the trapping of the fluid in the cavities between the rough elements, resulting in thicker thermal BLs and lower heat transfer efficiency. We depict in Fig. 3 the typical flow snapshots in the presence of the ratchet roughness of the aspect ratio $\gamma = 2$ in case B for increasing the value of Ra, showing the instantaneous temperature fields superimposed with the velocity vectors, particularly focusing on the boundary-layer region. As shown in Fig. 3(a), at low values of Ra, the thermal BL is thick and the boundary-layer flow in the cavities between the rough elements is weak and dominated by viscous effects.

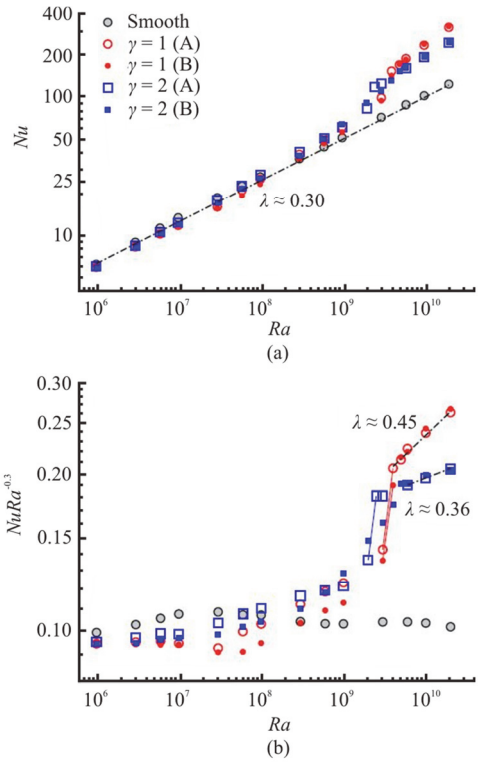

Fig. 2 (Color online) (a) The Nusselt number Nu as a function of Ra in convection cells with and without ratchet roughness. (b) The compensated plot of (a). The effective scaling behaviors of $Nu \sim Ra^{\lambda}$ are indicated by the dashed-dot lines. The red and blue solid lines in panel (b) indicate sharp jumps of the Nu value as the value of Ra is slightly increased for the roughness aspect ratio $\gamma = 1, 2$, respectively

As the value of Ra increases, the thermal BL becomes thinner, and the interaction between the BL flow and the roughness is stronger. With a thinner BL, secondary vortices are formed in the cavity regions between neighboring rough elements, which can result in more efficient fluid mixing, as shown in Fig. 3(c). This change of the flow structure is accompanied with a heat transfer enhancement compared with the smooth case at higher values of Ra, as shown in Fig. 2. Note that due to the complex flow organization consisting of a LSC and corner rolls, the BL properties are not uniform along the roughness surface. For the roughness height $h = 0.0625$, the transition from the Nu value reduction to the Nu value enhancement occurs at a critical Rayleigh number $Ra_c \sim O(10^8)$, which is quite close to the value of Ra_c in the case of the symmetric roughness with a comparable height, despite of the slight tilt of the convection cell in the present study and the Pr effect[17-18].

Interestingly, the heat transfer efficiencies for the four roughness configurations considered are close to each other at low enough values of Ra, demonstrating the insensitivity of the heat transport properties to the roughness geometry when the rough elements are deeply immersed inside the BLs. For higher values of Ra, the influence of the roughness geometry on the heat transfer becomes more prominent. In a Ra interval of more than one decade, the heat transfer efficiency in case A is better than that in case B for both roughness aspect ratios. This dependence of the heat transfer on the ratchet orientation is attributed to the difference of the flow organizations, which will be discussed below. It has been shown that the value of Ra_c for the onset of the Nu-enhanced regime is strongly dependent on both the roughness height and the value of Pr [17-18]. The results in the present study demonstrate that the changes of the roughness geometry and the ratchet orientation can result in a slight variation of the values of Ra_c for a fixed roughness height and a fixed value of Pr, as shown in Fig. 2.

As the value of Ra is further increased, the heat transfer enhancement becomes even more prominent as manifested by the steeper local scaling of the $Nu(Ra)$ relation in the rough cases. Figure 3(d) shows that at high enough values of Ra, the thermal

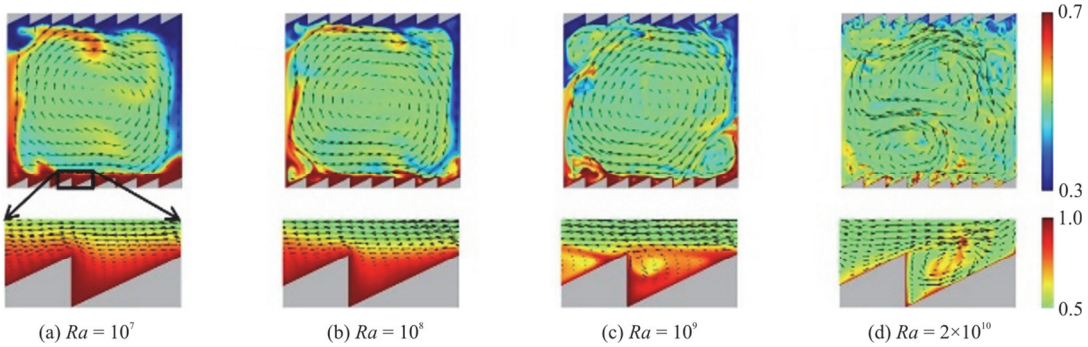

Fig. 3 (Color online) The instantaneous temperature fields superimposed with velocity vectors in the case with the roughness of aspect ratio $\gamma = 2$ in case B. The panels in the second row show the boundary-layer flows near the bottom plate

BL is evenly attached on the roughness surfaces, and the thermal plumes can be ejected from both the roughness tips and surfaces. The simulations show that for low and medium values of Ra, the instantaneous flow field consists of a well-organized, stable LSC (see Figs. 3(a)-3(c)), while at high enough values of Ra, the large-scale flow structure becomes less organized (see Fig. 3(d)). Despite that, a LSC can be clearly identified in the mean field.

To further demonstrate the influence of the ratchet roughness on the flow structure, we show in Fig. 4 the time-averaged flow fields in the smooth case, cases A, B at three different values of Ra. In the smooth case, the mean flow consists of a LSC and two smaller corner rolls. The corner rolls are formed through the plume detachment from the thermal BLs. Entrained by the LSC, the thermal plumes move up and down mainly along the sidewalls. In the presence of the ratchet roughness, while the LSC still exists and is on the whole unchanged for the parameters shown, the structure of the corner rolls can be significantly influenced. This is attributed to the fact that the corner rolls are less energetic than the LSC and of a comparable length scale with the roughness. By dramatically changing the boundary- layer flows, the roughness can strongly affect the formation and the structure of the corner rolls.

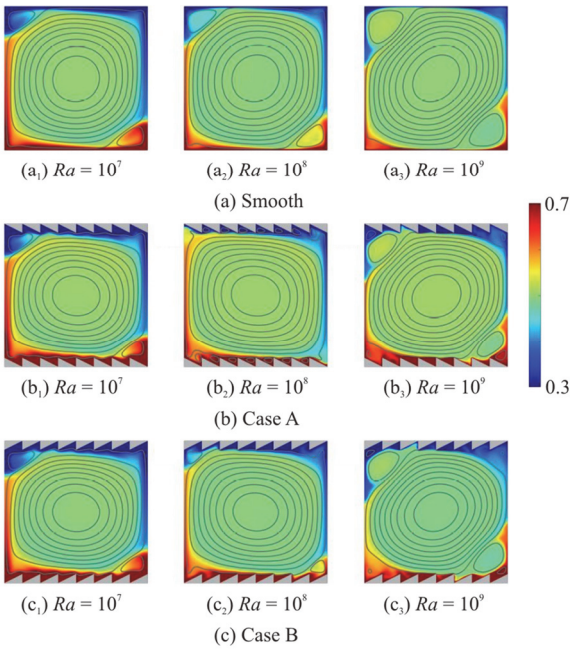

Fig. 4 (Color online) Time-averaged temperature fields superimposed with mean streamlines with $\gamma = 2$ at different values of Ra

When Ra takes a low value, the corner rolls are only mildly affected by the roughness, as shown in Figs. 4(a_1), 4(b_1), 4(c_1). This is due to the fact that the BLs are thick and the corner rolls are insensitive to the topography of the horizontal boundary, as is consistent with the heat transfer property that at low values of Ra the Nusselt numbers for different roughness configurations take similar values (see Fig. 2). For higher values of Ra, it is found that the corner rolls are suppressed due to the roughness (see Figs. 4(a_2), 4(b_2), 4(c_2)). Particularly, in Fig. 4(b_2) the corner rolls are completely suppressed, while in case B at the same value of Ra, the size of the corner rolls is smaller than that in the smooth case and is comparable to the horizontal length l of the roughness. The suppression of the corner rolls is attributed to the stronger disruption of the corner-roll flow by the roughness when the BLs become thinner. The difference between cases A, B originates from the fact that the component of the buoyancy force along the sloping surface of the ratchet roughness will, respectively, suppress and promote the formation of the anti-clockwise corner rolls in cases A, B. In Fig. 4(b_2), due to the complete suppression of the corner rolls, the plumes traveling along the sidewalls can directly impact the opposite boundary, making the BLs thinner in the impact regions as compared with case B in Fig. 4(c_2). At such intermediate values of Ra, the BLs on the roughness surfaces are highly non-uniform, as shown in the mean temperature fields in Fig. 4.

As the value of Ra is further increased, due to the stronger buoyancy effect and the presence of more plumes, the corner rolls become more energetic, as manifested in the larger scale of the corner rolls in Fig. 4(a_3) as compared with the cases at smaller values of Ra. At such large values of Ra, the strong corner rolls still exist in the presence of the roughness. However, each corner roll is divided into two circulating rolls of different sizes, which is reminiscent to the viscous eddies near a sharp corner[26]. In our case, the sequence of the corner rolls is promoted by the geometric modulation of the roughness.

Further examination of the Nu data in Fig. 2 reveals the presence of sharp jumps of the Nu value in the rough cases at relatively large values of Ra, which are marked by the solid lines in Fig. 2(b). During the Nu jump, a slight increase of the Ra value results in a huge enhancement of the heat transfer. The Nu jump is associated with a dramatic change of the flow structure, and the flow fields before and after the jump are characterized by distinctly different statistical properties. As an example, we plot in Figs. 5(a_1), 5(a_2) the temperature snapshots superimposed with the velocity vectors in a cell with roughness of aspect ratio $\gamma = 1$ in case A at two Rayleigh numbers $Ra = 3.0\times10^9$, 4.0×10^9, before and after the Nu jump. Besides the flow field, it is

also instructive to examine the distribution of the thermal dissipation rate $\varepsilon_T = \kappa \sum_i [\partial T(\boldsymbol{x},t)/\partial x_i]^2$, where κ is the thermal diffusivity of the working fluid. For the parameters considered, ε_T is dominated by the thermal BLs and the plumes[1]. The distributions of the time-averaged thermal dissipation rate $\langle \varepsilon_T \rangle_t$ are shown in Figs. 5(b_1), 5(b_2), where $\langle \cdot \rangle_t$ denotes the time averaging. Figure 5(a_1) shows that at $Ra = 3\times10^9$ before the Nu jump, the instantaneous flow field consists of a well-developed LSC and two corner rolls. The flow organization can also be inferred from the distribution of $\langle \varepsilon_T \rangle_t$ in Fig. 5(b_1). As expected, the large thermal dissipation rate is observed in the thermal BLs on the top and bottom plates and around the LSC and the corner rolls due to the plume dynamics. Interestingly, the distribution of the thermal dissipation rate near the horizontal plate is highly non-uniform. The thermal dissipation rate is evidently smaller in the cavities between the roughness in the central region of each horizontal plate, where the plume emission is also weaker.

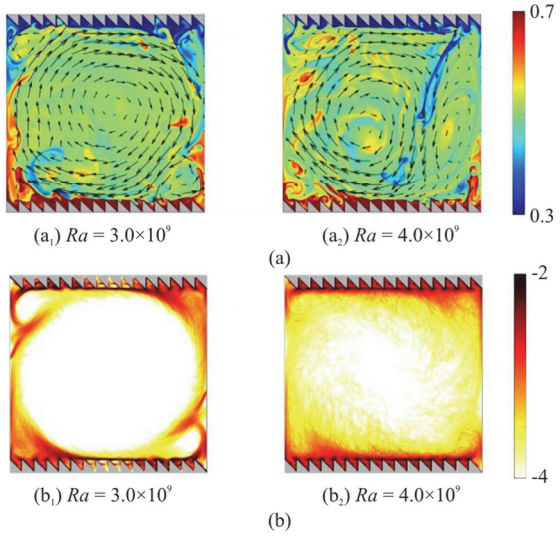

Fig. 5 (Color online) (a) The instantaneous temperature fields superimposed with velocity vectors, (b) the logarithm of time-averaged thermal dissipation rate $\lg(\langle \varepsilon_T \rangle_t)$ in a cell with roughness of aspect ratio $\gamma = 1$ in case A, before and after the Nu jump, respectively

At a slightly higher value of $Ra = 4.0\times10^9$, the heat transfer is enhanced by 56%. The instantaneous flow field in Fig. 5(a_2) shows that the large-scale flow structure becomes less organized and the secondary rolls at the top-left and bottom-right corners are not visible. The plumes detached from the thermal BLs can penetrate into the center core, as is different from the flow state shown in Fig. 5(a_1) at a lower value of Ra. To further quantify the change of the plume dynamics, we obtain the probability density functions (PDFs) of temperature fluctuation $\delta T = T - T_m$ in the bulk for the two cases, where T_m is the arithmetic mean temperature. The results are shown in Fig. 6(a). It is found that the temperature fluctuation at $Ra = 4.0\times10^9$ is significantly stronger than that at the slightly lower value of $Ra = 3.0\times10^9$. As the thermal plumes contribute to the large temperature fluctuation in the bulk, the huge enhancement of the temperature fluctuation confirms the dramatic change of the plume dynamics beyond the Nu jump.

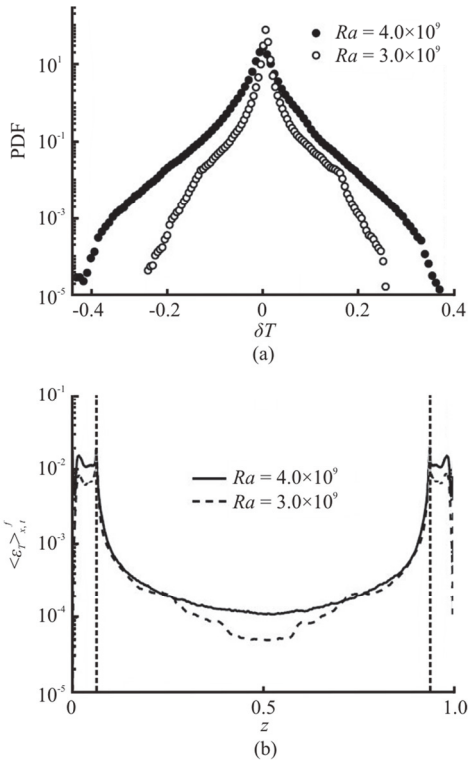

Fig. 6 Statistical properties of temperature fluctuation and thermal dissipation rate in the two cases shown in Fig. 5 in a cell with the roughness of aspect ratio $\gamma = 1$ in case A at $Ra = 3.0\times10^9$, 4.0×10^9. (a) The PDF of temperature fluctuation δT of the core flow inside a circular domain of radius $R/H = 0.4$. (b) Horizontally and temporally averaged thermal dissipation rate $\langle \varepsilon_T \rangle_{x,t}^f$ as a function of z. The vertical dashed lines indicate the tip positions of the roughness on the top and bottom surfaces

The change of the plume dynamics also suggests a change of the boundary layer property. This is manifested in the different distributions of the thermal dissipation rate in Figs. 5(b_1), 5(b_2). Compared with the lower-Ra case in Fig. 5(b_1), the distribution of $\langle \varepsilon_T \rangle_t$ in Fig. 5(b_2) is more uniform near each

horizontal plate. In the center part of the boundary-layer region, $\langle \varepsilon_T \rangle_t$ is increased and the plume emission is enhanced, which is attributed to the different large-scale flow structure in the bulk. Besides, the thermal dissipation in the bulk is enhanced due to the change of the plume dynamics. To further quantify the change of the dissipation properties during the Nu jump, we obtain the horizontally and temporally averaged thermal dissipation rate $\langle \varepsilon_T \rangle_{x,t}^f$, where $\langle \cdot \rangle_{x,t}^f$ denotes horizontal and temporal averaging over the fluid phase. The results are depicted in Fig. 6(b). As is consistent with the observation from Figs. 5(b_1), 5(b_2), the thermal dissipation rate is increased both in the bulk and in the boundary-layer region beyond the Nu jump. Thus, the Nu jump is associated with the dramatic change of the flow structure and the plume dynamics. Note that the Nu jump is not observed in the cell with the roughness of aspect ratio $\gamma = 2$ in case B, showing that the orientation of the ratchet roughness and the roughness geometry could significantly affect the flow state transition.

For the highest Rayleigh numbers considered in this study, the Nu data in Fig. 2 show that the presence of the roughness results in a much better heat transfer efficiency and a steeper Nu-Ra scaling as compared with the smooth case. At $Ra \sim O(10^{10})$, the value of Nu follows a local scaling law $Nu \sim Ra^{\lambda}$ with exponents $\lambda \approx 0.45$, $\lambda \approx 0.36$ for the two aspect ratios $\gamma = 1$, $\gamma = 2$, respectively. The dependence of the effective scaling exponent of the $Nu(Ra)$ relation in a rough cell on the aspect ratio of the roughness was reported in literature[12-13]. For $\gamma = 1$, $\lambda \approx 0.45$ is much larger than the value $\lambda \approx 0.30$ in the smooth case. It is of interest to further examine the effects of the roughness on the flow behavior. We plot in Figs. 7(a), 7(b) the vertical profiles of the time-averaged temperature $\langle T \rangle_t$ and the horizontal velocity $\langle u \rangle_t$ at $Ra = 2.0 \times 10^{10}$ in both smooth and rough cases. These profiles are taken at the center part of the boundary-layer region near the bottom plate, as described in the caption of Fig. 7. Both the temperature and velocity profiles show that the local flow details in the cavity between the roughness are different from the typical boundary-layer flow in the smooth case and dependent on the roughness aspect ratio and the ratchet orientation. At such high values of Ra, due to the interaction between the bulk flow and the roughness, the secondary vortices are formed in the cavities between the roughness, helping the fluid mixing in the boundary-layer region, as shown in the time-averaged flow fields in the inset of Fig. 7(b). We depict in the inset of Fig. 7(a) the temporally and horizontally averaged temperature profiles, which further demonstrate the great changes of the boundary-layer flows due to the roughness and the dependence of the flow details on the roughness aspect ratio in the global or averaged sense.

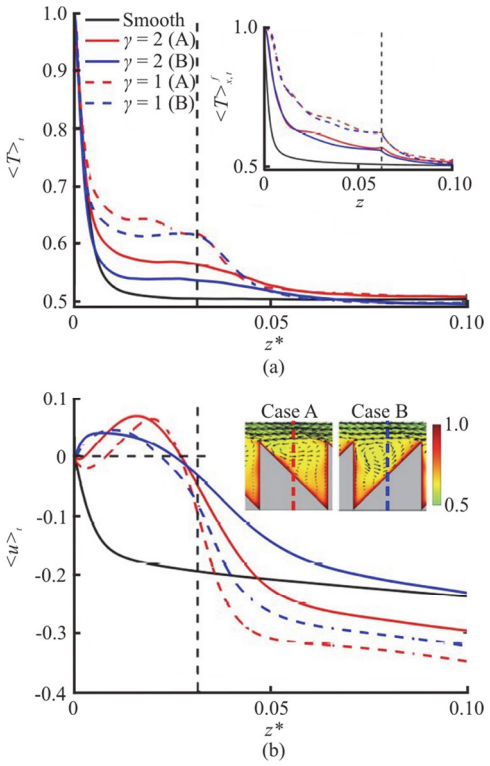

Fig. 7 (Color online) Time-averaged profiles of (a) temperature $\langle T \rangle_t$ and (b) horizontal velocity $\langle u \rangle_t$ along vertical sections $x = x_0$ for $Ra = 2.0 \times 10^{10}$ and for different roughness configurations. The horizontal variable $z^* = z - h_0$, where h_0 is the local roughness height at $x = x_0$. In the smooth case, $x_0 = 0.5$, $h_0 = 0$. In the cases $\gamma = 1$, 2, x_0 is, respectively, chosen to be $7.5 \times l(\gamma = 1) = 0.469$ (indicated by the vertical dashed lines in the inset of panel (b)) and $3.5 \times l(\gamma = 2) = 0.438$, such that we have $h_0 = h/2$ in both cases. The vertical dashed lines denote the vertical position of the roughness tip $z^* = h - h_0$. The inset of panel (a) shows the temporally and horizontally averaged temperature profiles $\langle T \rangle_{x,t}^f$ as functions of z. The vertical dashed lines denote the vertical position of the roughness tip $z = h$. The inset of panel (b) shows the time-averaged boundary-layer flows in a cavity between the roughness of aspect ratio $\gamma = 1$ near the center of the bottom plate

3. Conclusions

In summary, we have carried out a numerical study of the two-dimensional RBC over ratchet surfaces, covering the Ra range $1.0\times10^6 \le Ra \le 2.0\times10^{10}$ at a fixed $Pr = 4$. We consider two aspect ratios of the roughness γ = 1, 2, with a fixed roughness height $h/H = 0.0625$. The LSC is locked in the clockwise direction through an inclination of the convection cell by a small angle $\beta = 6°$.

This study is focused on the effects of the ratchet roughness on the heat transfer and the flow structure of the RBC. At low enough values of Ra, the heat transfer is found to be insensitive to the roughness geometry, the influence of which becomes more prominent at higher values of Ra with thinner BLs. As the value of Ra is increased from a low level, a transition from the Nu reduction to the Nu enhancement is observed, and the critical Rayleigh number Ra_c for this transition is mildly changed for different aspect ratios and orientations of the ratchet roughness. We find that the roughness can have a significant effect on the organization of the corner rolls, which are evidently suppressed for intermediate values of Ra.

A sharp jump of Nu is identified in the case with the roughness, accompanied with the dramatic changes of the large-scale flow structure and the plume dynamics. At high values of Ra, the thermal BLs are evenly attached on the roughness surfaces. An examination of the boundary-layer flows shows that complex secondary vortices are developed in the cavities between the roughness, and the flow behavior with the roughness is different from the typical laminar BLs of the classical RBC in the smooth case in both local and global sense.

It is of interest to study the sensitivity of the system response to the small tilting angle. We focus on the specific case of the convection with the roughness of aspect ratio $\gamma = 2$, and compare the reported results for $\beta = 6°$ with those for a smaller tilting angle of 3° at selected values of Ra. It is found that the change of the tilting angle has only mild influences on the flow behavior. Particularly, the relative differences of the values of Nu between the two cases with different values of β are small (within 3% for the considered Ra values), the sharp jump of Nu is on the whole unchanged as β is decreased from 6° to 3°, and the effects of the ratchet roughness on the flow structure are consistent for the two different tilting angles. Thus, it is expected that the main conclusions of this study are robust to a slight change of the small tilting angle. In the future, it will be of interest to systematically study the effects of tilting on the turbulent convection over rough surfaces for a wide range of tilting angles.

References

[1] Ahlers G., Grossmann S., Lohse D. Heat transfer and large scale dynamics in turbulent Rayleigh-Bénard convection [J]. *Reviews of Modern Physics*, 2009, 81(2): 503-537.

[2] Lohse D., Xia K. Q. Small-scale properties of turbulent Rayleigh-Bénard convection [J]. *Annual Review of Fluid Mechanics*, 2010, 42: 335-364.

[3] Chilla F., Schumacher J. New perspectives in turbulent Rayleigh-Bénard convection [J]. *The European Physical Journal E*, 2012, 35(7): 58.

[4] Xia K. Q. Current trends and future directions in turbulent thermal convection [J]. *Theoretical and Applied Mechanics Letters*, 2013, 3(5): 052001.

[5] Shen Y., Tong P., Xia K. Q. Turbulent convection over rough surfaces [J]. *Physical Review Letters*, 1996, 76(6): 908-911.

[6] Du Y. B., Tong P. Enhanced heat transport in turbulent convection over a rough surface [J]. *Physical Review Letters*, 1998, 81(5): 987-990.

[7] Du Y. B., Tong P. Turbulent thermal convection in a cell with ordered rough boundaries [J]. *Journal of Fluid Mechanics*, 2000, 407: 57-84.

[8] Villermaux E. Transfer at rough sheared interfaces [J]. *Physical Review Letters*, 1998, 81(22): 4859-4862.

[9] Ciliberto S., Laroche C. Random roughness of boundary increases the turbulent convection scaling exponent [J]. *Physical Review Letters*, 1999, 82(20): 3998-4001.

[10] Roche P. E., Castaing B., Chabaud B. et al. Observation of the 1/2 power law in Rayleigh-Bénard convection [J]. *Physical Review E*, 2001, 63(4): 045303.

[11] Xie Y. C., Xia K. Q. Turbulent thermal convection over rough plates with varying roughness geometries [J]. *Journal of Fluid Mechanics*, 2017, 825: 573-599.

[12] Toppaladoddi S., Succi S., Wettlaufer J. S. Roughness as a route to the ultimate regime of thermal convection [J]. *Physical Review Letters*, 2017, 118(7): 074503.

[13] Zhu X., Stevens R. J. A. M., Verzicco R. et al. Roughness-facilitated local 1/2 scaling does not imply the onset of the ultimate regime of thermal convection [J]. *Physical Review Letters*, 2017, 119(15): 154501.

[14] Xu B. L., Wang Q., Wan Z. H. et al. Heat transport enhancement and scaling law transition in two-dimensional Rayleigh-Bénard convection with rectangular-type roughness [J]. *International Journal of Heat and Mass Transfer*, 2018, 121: 872-883.

[15] Zhu X., Stevens R. J. A. M., Shishkina O. et al. $Nu\sim Ra^{1/2}$ scaling enabled by multiscale wall roughness in Rayleigh-Bénard turbulence [J]. *Journal of Fluid Mechanics*, 2019, 869: R4.

[16] Toppaladoddi S., Wells A. J., Doering C. R. et al. Thermal convection over fractal surfaces [J]. *Journal of Fluid Mechanics*, 2021, 907: A12.

[17] Zhang Y. Z., Sun C., Bao Y. et al. How surface roughness reduces heat transport for small roughness heights in turbulent Rayleigh-Bénard convection [J]. *Journal of Fluid Mechanics*, 2018, 836: R2.

[18] Yang J. L., Zhang Y. Z., Jin T. C. et al. The *Pr*- dependence of the critical roughness height in two-dimensional turbulent Rayleigh-Bénard convection [J]. *Journal of Fluid Mechanics*, 2021, 911: A52.

[19] Jiang H., Zhu X., Mathai V. et al. Controlling heat transport and flow structures in thermal turbulence using ratchet surfaces [J]. *Physical Review Letters*, 2018, 120(4): 044501.
[20] Verzicco R., Orlandi P. A finite-difference scheme for three-dimensional incompressible flows in cylindrical coordinates [J]. *Journal of Computational Physics*, 1996, 123(2): 402-414.
[21] van der Poel E. P., Ostilla-Monico R., Donners J. et al. A pencil distributed finite difference code for strongly turbulent wall-bounded flows [J]. *Computers and Fluids*, 2015, 116: 10-16.
[22] Jiang H., Zhu X., Mathai V. et al. Convective heat transfer along ratchet surfaces in vertical natural convection [J]. *Journal of Fluid Mechanics*, 2019, 873: 1055-1071.
[23] Fadlun E. A., Verzicco R., Orlandi P. et al. Combined immersed-boundary finite-difference methods for three-dimensional complex flow simulations [J]. *Journal of Computational Physics*, 2000, 161(1): 35-60.
[24] Shishkina O., Stevens R. J. A. M., Grossmann S. et al. Boundary layer structure in turbulent thermal convection and its consequences for the required numerical resolution [J]. *New Journal of Physics*, 2010, 12(7): 075022.
[25] Zhang Y., Zhou Q., Sun C. Statistics of kinetic and thermal energy dissipation rates in two-dimensional turbulent Rayleigh-Bénard convection [J]. *Journal of Fluid Mechanics*, 2017, 814: 165-184.
[26] Moffatt H. K. Viscous and resistive eddies near a sharp corner [J]. *Journal of Fluid Mechanics*, 1964, 18: 1-18.

Appendix

We list in Table A1 the numerical details for all the simulations in both the smooth and rough cases.

Table A1 Numerical details for all the simulations in both the smooth and rough cases. The columns from left to right are the Rayleigh number Ra, the grid resolution (N_x, N_z) and Nu in the smooth case, the rough case with $\gamma = 1$, and the rough case with $\gamma = 2$ (indicated by the subscript)

Ra	$(N_x, N_z)_{\text{smooth}}$	Nu_{smooth}	$(N_x, N_z)_{\gamma=1}$	$Nu_{\gamma-1,\text{case A}}$	$Nu_{\gamma-1,\text{case B}}$	$(N_x, N_z)_{\gamma-2}$	$Nu_{\gamma-2,\text{case A}}$	$Nu_{\gamma=2,\text{case B}}$
10^6	180×180	6.258	256×256	5.958	6.013	256×256	6.014	5.952
3.0×10^6	180×180	9.008	256×256	8.341	8.264	256×256	8.499	8.292
6.0×10^6	180×180	11.40	256×256	10.32	10.15	256×256	10.66	10.40
10^7	256×256	13.54	256×256	11.91	11.85	256×256	12.39	12.17
3.0×10^7	256×256	19.00	256×256	16.21	15.92	256×256	18.12	17.22
6.0×10^7	384×384	23.10	384×384	21.47	19.64	384×384	23.19	21.93
10^8	384×384	26.90	384×384	25.87	23.78	384×384	27.71	26.11
3.0×10^8	512×512	36.35	512×512	39.21	36.12	512×512	40.67	38.47
6.0×10^8	512×512	44.33	768×768	51.05	46.98	768×768	51.32	50.91
10^9	512×512	51.63	768×768	61.91	56.67	768×768	61.03	64.62
2.0×10^9	-	-	-	-	-	1 280×1 280	84.41	92.03
2.5×10^9	-	-	-	-	-	1 280×1 280	119.6	-
3.0×10^9	768×768	72.40	1 280×1 280	99.79	95.06	1 280×1 280	126.2	112.3
4.0×10^9	-	-	1 800×1 800	155.3	144.2	1 800×1 800	-	132.4
5.0×10^9	-	-	1 800×1 800	172.4	174.3	1 800×1 800	-	155.4
6.0×10^9	1 024×1 024	89.14	1 800×1 800	191.3	188.6	1 800×1 800	163.2	163.9
10^{10}	1 024×1 024	103.4	1 800×1 800	238.7	243.4	1 800×1 800	195.5	198.4
2.0×10^{10}	1 280×1 280	125.2	2 560×2 560	321.6	326.6	2 048×2 048	250.8	250.1